The Journal of Chemical Physics

Speeding-up *ab initio* molecular dynamics with hybrid functionals using adaptively compressed exchange operator based multiple timestepping

Cite as: J. Chem. Phys. **151**, 151102 (2019); https://doi.org/10.1063/1.5125422
Submitted: 22 August 2019 . Accepted: 01 October 2019 . Published Online: 17 October 2019

Sagarmoy Mandal, and Nisanth N. Nair

View Online Export Citation CrossMark

ARTICLES YOU MAY BE INTERESTED IN

Exploring local range separation: The role of spin scaling and one-electron self-interaction
The Journal of Chemical Physics **151**, 154108 (2019); https://doi.org/10.1063/1.5121731

In search of Coulson's lost theorem
The Journal of Chemical Physics **151**, 151101 (2019); https://doi.org/10.1063/1.5128624

Force balance approach for advanced approximations in density functional theories
The Journal of Chemical Physics **151**, 154107 (2019); https://doi.org/10.1063/1.5123608

Challenge us.
What are your needs for periodic signal detection?
Zurich Instruments
Watch

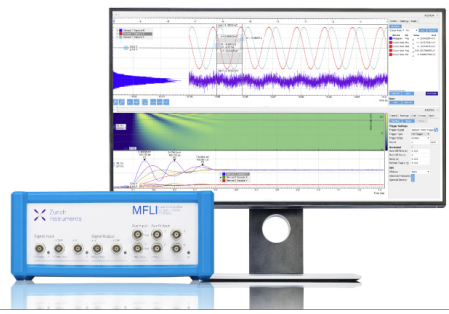

AIP Publishing

© 2019 Author(s).

The Journal of Chemical Physics | COMMUNICATION | scitation.org/journal/jcp

Speeding-up *ab initio* molecular dynamics with hybrid functionals using adaptively compressed exchange operator based multiple timestepping

Cite as: J. Chem. Phys. 151, 151102 (2019); doi: 10.1063/1.5125422
Submitted: 22 August 2019 • Accepted: 1 October 2019 •
Published Online: 17 October 2019

View Online Export Citation CrossMark

Sagarmoy Mandal and Nisanth N. Nair[a)]

AFFILIATIONS

Department of Chemistry, Indian Institute of Technology Kanpur, Kanpur 208016, India

[a)]Electronic mail: nnair@iitk.ac.in

ABSTRACT

Ab initio molecular dynamics (AIMD) simulations using hybrid density functionals and plane waves are of great interest owing to the accuracy of this approach in treating condensed matter systems. On the other hand, such AIMD calculations are not routinely carried out since the computational cost involved in applying the Hartree–Fock exchange operator is very high. In this work, we make use of a strategy that combines adaptively compressed exchange operator formulation and multiple time step integration to significantly reduce the computational cost of these simulations. We demonstrate the efficiency of this approach for a realistic condensed matter system.

Published under license by AIP Publishing. https://doi.org/10.1063/1.5125422

Ab initio molecular dynamics (AIMD) simulations with density functional theory (DFT) and plane wave (PW) basis set are the methods of choice in studying the structural and dynamic properties of condensed matter systems.[1] Usage of density functionals at the level of the Generalized Gradient Approximation (GGA) is commonplace for these simulations because more than a million energy and force evaluations are computationally achievable by taking advantage of parallel programs and parallel computing platforms. Contrarily, hybrid density functionals are preferred over GGA functionals for improved accuracy in AIMD simulations.[2–5] Computations of energy and gradients at the hybrid functional level using the PW basis set have prohibitively high computational cost resulting from the application of the exact exchange operator on each of the occupied orbitals. One of the ways to increase the efficiency of such AIMD simulations is by making use of multiple time step (MTS) algorithms[6,7] among others.[4,8–13] In this respect, the reversible reference system propagator algorithm (r-RESPA)[7] has been used by several authors.[14–16] In the r-RESPA MTS approach, artificial time scale separation in the ionic force components due to the computationally intensive Hartree–Fock exchange (HFX) contribution and the computationally cheaper rest of the terms is made.[14,15] In this manner, the MTS scheme allows us to compute HFX contributions less frequently compared to the rest of the contributions to the force, thereby reducing the overall computational cost in performing AIMD simulations.

Here, we propose a new way to take advantage of the r-RESPA scheme for performing AIMD using hybrid functionals and PWs. This scheme is based on the recently developed adaptively compressed exchange (ACE) operator approach.[17,18] We exploited some property of the ACE operator to artificially split the ionic forces into fast and slow.

The self-consistent field (SCF) solution of hybrid functional based Kohn-Sham (KS) DFT equations requires application of the exchange operator $\mathbf{V}_X = -\sum_j^{N_{orb}} \frac{|\psi_j\rangle\langle\psi_j|}{r_{12}}$ on each of the KS orbitals $|\psi_i\rangle$,

$$\mathbf{V}_X|\psi_i\rangle = -\sum_j^{N_{orb}} |\psi_j\rangle\langle\psi_j|(r_{12})^{-1}|\psi_i\rangle, \quad i = 1,\ldots,N_{orb}. \tag{1}$$

Here, N_{orb} is the total number of occupied orbitals. The evaluation of $\langle\psi_j|(r_{12})^{-1}|\psi_i\rangle$ is usually done in reciprocal space[8,19] using Fourier

Published under license by AIP Publishing

transform (FT). If N_G is the total number of PWs, the computational cost for doing FT scales as $N_G \log N_G$ on using the fast Fourier transform (FFT) algorithm. The total computational cost scales as $N_{orb}^2 N_G \log N_G$,[19] as operation of $\mathbf{V}_X$ on all the KS orbitals requires N_{orb}^2 time evaluation of $\langle\psi_j|(r_{12})^{-1}|\psi_i\rangle$.

In the recently developed ACE operator formulation,[17] the full rank $\mathbf{V}_X$ operator is approximated by the ACE operator $\mathbf{V}_X^{ACE} = -\sum_k^{N_{orb}} |P_k\rangle\langle P_k|$ using a low rank decomposition. Here, $\{|P_k\rangle\}$ is the set of ACE projection vectors which can be computed through a series of simpler linear algebra operations, as explained below.

In matrix notation, $\mathbf{V}_X^{ACE}$ can be rewritten as

$$\mathbf{V}_X^{ACE} = \mathbf{P}\mathbf{P}^T, \tag{2}$$

with $\{|P_k\rangle\}$ being columns of $\mathbf{P}$. Here,

$$\mathbf{P} = \mathbf{W}\mathbf{L}^{-T}, \tag{3}$$

where the columns of $\mathbf{W}$ are

$$|W_i\rangle = \mathbf{V}_X|\psi_i\rangle, \quad i = 1, \ldots, N_{orb}. \tag{4}$$

$\mathbf{L}$ is a lower triangular matrix computed using the Cholesky factorization of $-\mathbf{M}$ as

$$\mathbf{M} = -\mathbf{L}\mathbf{L}^T. \tag{5}$$

Here, the elements of the matrix $\mathbf{M}$ are

$$M_{kl} = \langle\psi_k|\mathbf{V}_X|\psi_l\rangle. \tag{6}$$

The evaluation of the action of the $\mathbf{V}_X^{ACE}$ operator on KS orbitals can be done with the N_{orb}^2 number of inner products as

$$\mathbf{V}_X^{ACE}|\psi_i\rangle = -\sum_k^{N_{orb}} |P_k\rangle\langle P_k|\psi_i\rangle, \quad i = 1, \ldots, N_{orb}. \tag{7}$$

The advantage of the ACE approach is that the cost of applying the $\mathbf{V}_X^{ACE}$ operator on each KS orbitals is much less as compared to the $\mathbf{V}_X$ operator. At the first SCF step, the $\mathbf{V}_X^{ACE}$ operator can be constructed through the computation of $\{\mathbf{V}_X|\psi_i\rangle\}$, which is the costliest step [because of N_{orb}^2 time evaluation of $\langle\psi_j|(r_{12})^{-1}|\psi_i\rangle$]. As HFX has only a minor contribution to the total energy, an approximate energy computation is possible by using the previously constructed $\mathbf{V}_X^{ACE}$ operator without updating it for the rest of the SCF iterations. It is again stressed that once the $\mathbf{V}_X^{ACE}$ operator is constructed, its low rank structure allows the easy computation of $\{\mathbf{V}_X^{ACE}|\psi_i\rangle\}$ in the subsequent SCF iterations. We exploit this property of the ACE operator to combine with the r-RESPA scheme.

In the r-RESPA method,[7] symmetric Trotter factorization of the classical time evolution operator is carried out. Let that ionic force can be decomposed into slow and fast components as $F_K = F_K^{fast} + F_K^{slow}$, $K = 1, \ldots, 3N$, for a system containing N atoms. In this case, the Liouville operator L can be written as

$$iL = iL_1^{fast} + iL_2^{fast} + iL^{slow}, \tag{8}$$

with

$$iL_1^{fast} = \sum_{K=1}^{3N}\left[\dot{X}_K \frac{\partial}{\partial X_K}\right], \quad iL_2^{fast} = \sum_{K=1}^{3N}\left[F_K^{fast}\frac{\partial}{\partial P_K}\right] \tag{9}$$

and

$$iL^{slow} = \sum_{K=1}^{3N}\left[F_K^{slow}\frac{\partial}{\partial P_K}\right]. \tag{10}$$

Here, $\{X_K\}$ and $\{P_K\}$ are the Cartesian coordinates and the conjugate momenta of the particles, respectively. Using symmetric Trotter factorization, we arrive at

$$\exp(iL\Delta t) \approx \exp\left(iL^{slow}\frac{\Delta t}{2}\right)\left[\exp\left(iL_2^{fast}\frac{\delta t}{2}\right)\exp\left(iL_1^{fast}\delta t\right) \times \exp\left(iL_2^{fast}\frac{\delta t}{2}\right)\right]^n \exp\left(iL^{slow}\frac{\Delta t}{2}\right). \tag{11}$$

Here, the large time step Δt is chosen according to the time scale of variation of slow forces ($\{F_K^{slow}\}$) and the smaller time step $\delta t = \Delta t/n$ is chosen according to the time scale of fast forces ($\{F_K^{fast}\}$).

Now, we split the contribution of ionic forces from the HFX part as

$$F_K^{hybrid} = F_K^{ACE} + \Delta F_K, \quad K = 1, \ldots, 3N, \tag{12}$$

with $\Delta F_K = \left(F_K^{hybrid} - F_K^{ACE}\right)$. Here, $\mathbf{F}^{hybrid}$ is the ionic force computed with the full rank exchange operator $\mathbf{V}_X$. The term $\mathbf{F}^{ACE}$ is the ionic force calculated using the low rank $\mathbf{V}_X^{ACE}$ operator. In our approach, we invoke the approximation that $\mathbf{F}^{fast} \equiv \mathbf{F}^{ACE}$ and $\mathbf{F}^{slow} \equiv \Delta\mathbf{F}$. Here, the longer time step Δt is chosen according to the time scale of variation of the computationally costly slow forces ($\Delta\mathbf{F}$), whereas the smaller time step δt is taken as per the time scale of fast forces that are cheaper to compute ($\mathbf{F}^{ACE}$). In this way, we get the required speed-up using the r-RESPA scheme to perform hybrid functional based AIMD simulations.

In Figs. 1(a) and 1(b), we have shown the components of the $\mathbf{F}^{ACE}$ and $\Delta\mathbf{F}$ for a realistic molecular system, where $\mathbf{V}_X^{ACE}$ is calculated once at the beginning of a SCF while kept fixed during the remaining SCF cycles and ΔF is calculated every $n = \Delta t/\delta t$ steps. The magnitude of $\Delta\mathbf{F}$ is ~100 times smaller compared to $\mathbf{F}^{ACE}$ (see the supplementary material). Moreover, $\Delta\mathbf{F}$ computed at every $n = \Delta t/\delta t$ steps is slowly varying. Thus, the artificial time scale separation considered here is reasonable. We emphasize that it is practically difficult to have $\Delta\mathbf{F}$ resonance-free and thus the total energy conservation may not be fully satisfied. In such cases, efficient thermostats have to be used while performing canonical ensemble simulations to avoid long time energy drifts.[20] We note in passing that force-splitting done by differences in forces due to two levels of theory as in Ref. 15 has larger amplitude of oscillation than $\Delta\mathbf{F}$ constructed using the ACE approach (see the supplementary material). Flowcharts of the method are given in Figs. 2 and 3.

Benchmark calculations were carried out for a 32 water system where the molecules were taken in a supercell of dimensions 9.85 Å × 9.85 Å × 9.85 Å with water density ~1 g cm^{-3}. Calculations were carried out employing the CPMD program[21] where the proposed method has been implemented. The PBE0[22] exchange correlation functional was employed together with the norm-conserving Troullier-Martin type pseudopotentials.[23] A PW cutoff energy of 80 Ry was used. Born-Oppenheimer molecular dynamics (BOMD)

Published under license by AIP Publishing

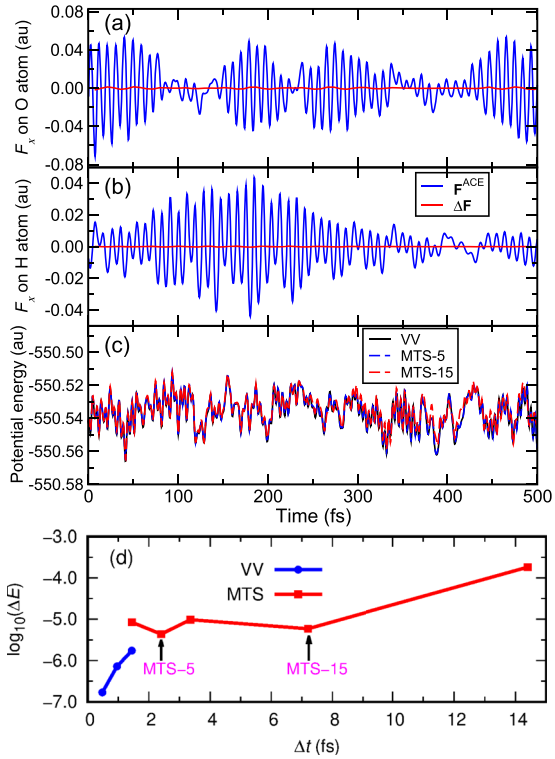

FIG. 1. Test results for the 32-water system using the PBE0 functional: one of the components of $\mathbf{F}^{ACE}$ and $\Delta\mathbf{F}$ on an arbitrarily chosen (a) oxygen and (b) hydrogen atoms. Here, $\mathbf{F}^{ACE}$ and $\Delta\mathbf{F}$ are calculated at every δt and Δt, respectively. (c) Comparison of potential energy during **VV**, **MTS-5**, and **MTS-15** simulations in the NVE ensemble. (d) $\log_{10}(\Delta E)$ for different Δt values in **VV** and **MTS** simulations calculated from 5 ps long trajectories.

simulations were carried out to perform MD simulations at the microcanonical (NVE) and canonical (NVT) ensembles. In order to perform the canonical ensemble AIMD simulation, we employed Nosé–Hoover chain thermostats[24] and the temperature of the system was set to 300 K. Addition of thermostats also helps to eliminate any resonance effects originated with the use of large time step.[20,25] At every MD steps, wavefunctions were converged until the magnitude of the maximum wavefunction gradient reached below 1×10^{-6} a.u. The initial guess for the wavefunctions at every MD step was obtained using the Always Stable Predictor Corrector Extrapolation scheme[26] of order 5.

To benchmark our implementation, we first compared the fluctuations in the total energy using the conventional velocity Verlet (**VV**) integrator and MTS runs (**MTS-n**) with $n = \Delta t/\delta t$, and $\delta t \approx 0.5$ fs for 32-water in a periodic box treated by the PBE0 functional. The magnitude of the total energy (E) fluctuations is measured by

$$\Delta E = \left\langle \left| \frac{E - \langle E \rangle}{\langle E \rangle} \right| \right\rangle, \tag{13}$$

where $\langle \cdots \rangle$ specifies the time average. In the case of **VV** runs, $\log_{10}(\Delta E)$ increases with higher Δt corresponding to the increase in total energy fluctuations as shown in Fig. 1(d). We also observed that

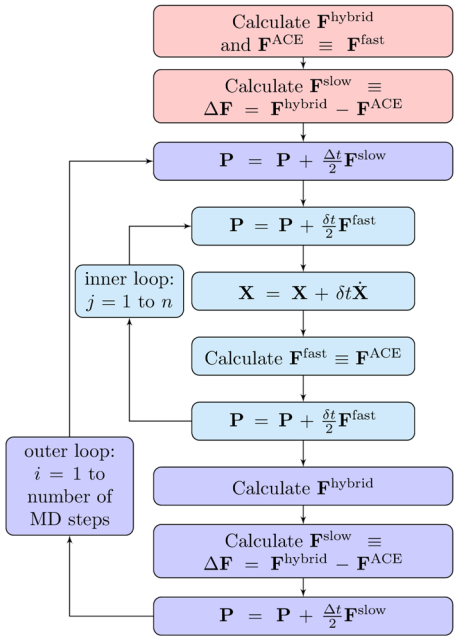

FIG. 2. Flowchart of the MTS propagation scheme proposed in this work.

the use of a time step greater than 1.4 fs in **VV** runs leads to unstable trajectories with breaking of O–H covalent bonds. In **MTS-n** runs, we kept the inner time step δt fixed at 0.5 fs and varied outer time step $\Delta t = n\,\delta t$. The quality of the energy conservation in these runs

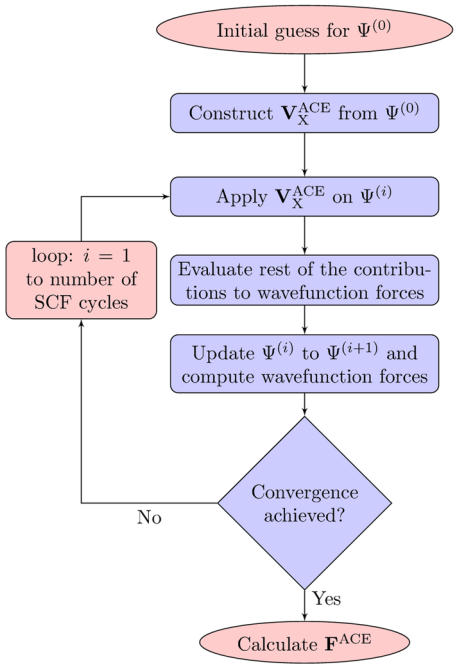

FIG. 3. Flowchart showing the steps involved in computing $\mathbf{F}^{ACE}$. Here, $\Psi^{(i)}$ is the wavefunction at the ith iteration.

Published under license by AIP Publishing

TABLE I. Comparison of various quantities for **VV**, **MTS-5**, and **MTS-15** simulations in the NVE ensemble.

Method	$\log_{10}(\Delta E)$[a]	ΔU/(a.u.)[b]	$t_{CPU}/(s)$[c]	Speed-up[d]
VV	−6.8	0.0	258	1
MTS-5	−5.4	5.9×10^{-4}	64	4
MTS-15	−5.2	1.9×10^{-3}	38	7

[a]Calculated using Eq. (13) over 5 ps long trajectories.
[b]The average absolute deviation of potential energy in **MTS-n** runs from the **VV** run: $\Delta U = \langle |U^{VV} - U^{MTS\text{-}n}| \rangle$. Here, $U^{VV/MTS-n}$ is the potential energy at any time during **VV**/**MTS-n** run. This average is calculated over 1000 MD steps.
[c]Average computational time per MD step (averaged over 500 MD steps) performed using identical 120 processors.
[d]Speed-up is the ratio of t_{CPU} for **VV** and **MTS-n** runs.

depends on the value of n, which determines how large the outer time step is compared to the inner time step. It is clear from Fig. 1(d) that **MTS-n** runs with n up to 15 have the total energy conservation comparable (to the order of magnitude) to the **VV** run using a time step 1.4 fs. Although the **MTS-30** run (with Δt = 14.4 fs) was showing higher total energy fluctuation, it was able to generate stable MD trajectories. Notably, we observed good accuracy in **MTS** runs with n = 15 (i.e., **MTS-15**) (see Table I). The total energy drifts for different NVE runs are reported in the supplementary material.

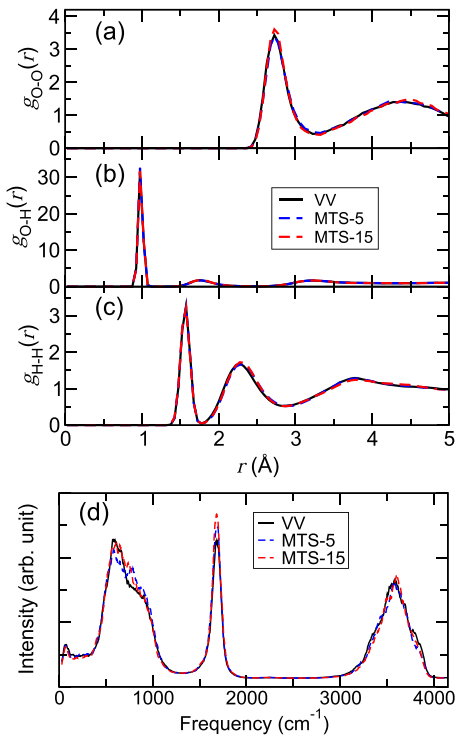

FIG. 4. Radial distribution functions (RDFs) for bulk water simulation from **VV**, **MTS-5**, and **MTS-15** trajectories at the level of PBE0: (a) O–O, (b) O–H, and (c) H–H. (d) Power spectrum of the same system computed from **VV**, **MTS-5**, and **MTS-15** trajectories.

TABLE II. CPU time for various stages of the program.

CPU time per SCF using the $\mathbf{V}_X$ operator	24 s
CPU time per SCF using the $\mathbf{V}_X^{ACE}$ operator	0.1 s
Average CPU time for the construction of $\mathbf{V}_X^{ACE}$ at the beginning of every MD step	24 s

In order to show the correctness of our proposed MTS scheme, we compared the fluctuation in potential energy for **VV**, **MTS-5**, and **MTS-15** runs for a short initial time period for the 32-water system (before the trajectories deviate due to growing numerical differences) in Fig. 1(c) (see also Table I). All these simulations were started with the same initial conditions. We find that potential energy computed from the **MTS-5** and **MTS-15** trajectories is closely following the potential energy from the **VV** run.

As the next, we carried out NVT simulations for the same system and computed the static and dynamical properties of bulk water. In particular, we calculated partial radial distribution functions (RDFs) and the power spectrum (see Fig. 4). It is clear that the RDFs from the **MTS** simulations are in excellent agreement with those from the **VV** run [Figs. 4(a)–4(c)]. In addition, the power spectrum computed from these calculations is in excellent agreement [Fig. 4(d)]. Thus, we conclude that our **MTS** scheme gives an accurate description of the structural and dynamical properties.

We now compare the average computational time per MD step (t_{CPU}) for **MTS-n** and **VV** runs (see Tables I and II). We have achieved a speed-up of ~4 fold for the 32-water system with **MTS-5** as compared to the **VV** run. At the same time, with **MTS-15**, we could achieve a speed-up of ~7 fold. We have observed a similar speed-up for larger system sizes (see the supplementary material). It is crucial to note that application of the $\mathbf{V}_X^{ACE}$ operator at every SCF cycle in place of the exact exchange operator $\mathbf{V}_X$ gives a speed-up of ~240 (see Table II). However, construction of the $\mathbf{V}_X^{ACE}$ operator, which is done only once in every MD time step, is computationally expensive (and has the same computational cost of applying the exact exchange operator). Thus in this method, construction of $\mathbf{V}_X^{ACE}$ remains as the computational bottleneck.

In conclusion, we presented a new scheme in using the r-RESPA to perform hybrid functional based AIMD simulations with the PW basis set. This involves artificial splitting in the nuclear forces envisaged by the recently developed ACE approach. Our benchmark results for liquid water show that stable and accurate MD trajectories can be obtained through this procedure. For the specific case of a 32-water system, a computational speed-up up to 7 could be obtained. We hope that this approach will enable us to compute long accurate AIMD trajectories at the level of hybrid DFT. Systematic improvements can be further made to speed up this approach, in particular, using localized orbitals for the construction of the ACE operator,[27] and by employing a resonance free thermostat,[20] while these are beyond the scope of this work.

Published under license by AIP Publishing

See the supplementary material for the comparison of fast and slow force components, total energy drift, and benchmark for larger system sizes.

The authors acknowledge the HPC facility at the Indian Institute of Technology Kanpur (IITK) for the computational resources. S.M. thanks the University Grant Commission (UGC), India, for his Ph.D. fellowship. S.M. is grateful to Mr. Banshi Das (IITK) for his help in generating the power spectrum.

REFERENCES

[1] D. Marx and J. Hutter, *Ab Initio Molecular Dynamics: Basic Theory and Advanced Methods* (Cambridge University Press, Cambridge, 2009).
[2] T. Todorova, A. P. Seitsonen, J. Hutter, I.-F. W. Kuo, and C. J. Mundy, J. Phys. Chem. B **110**, 3685 (2006).
[3] C. Zhang, D. Donadio, F. Gygi, and G. Galli, J. Chem. Theory Comput. **7**, 1443 (2011).
[4] R. A. DiStasio, Jr., B. Santra, Z. Li, X. Wu, and R. Car, J. Chem. Phys. **141**, 084502 (2014).
[5] F. Ambrosio, G. Miceli, and A. Pasquarello, J. Phys. Chem. B **120**, 7456 (2016).
[6] M. E. Tuckerman, G. J. Martyna, and B. J. Berne, J. Chem. Phys. **93**, 1287 (1990).
[7] M. Tuckerman, B. J. Berne, and G. J. Martyna, J. Chem. Phys. **97**, 1990 (1992).
[8] X. Wu, A. Selloni, and R. Car, Phys. Rev. B **79**, 085102 (2009).
[9] F. Gygi and I. Duchemin, J. Chem. Theory Comput. **9**, 582 (2013).
[10] W. Dawson and F. Gygi, J. Chem. Theory Comput. **11**, 4655 (2015).
[11] L. E. Ratcliff, A. Degomme, J. A. Flores-Livas, S. Goedecker, and L. Genovese, J. Phys.: Condens. Matter **30**, 095901 (2018).
[12] S. Mandal, J. Debnath, B. Meyer, and N. N. Nair, J. Chem. Phys. **149**, 144113 (2018).
[13] G. F. von Rudorff, R. Jakobsen, K. M. Rosso, and J. Blumberger, J. Chem. Theory Comput. **13**, 2178 (2017).
[14] M. Guidon, F. Schiffmann, J. Hutter, and J. VandeVondele, J. Chem. Phys. **128**, 214104 (2008).
[15] E. Liberatore, R. Meli, and U. Rothlisberger, J. Chem. Theory Comput. **14**, 2834 (2018).
[16] S. Fatehi and R. P. Steele, J. Chem. Theory Comput. **11**, 884 (2015).
[17] L. Lin, J. Chem. Theory Comput. **12**, 2242 (2016).
[18] W. Hu, L. Lin, A. S. Banerjee, E. Vecharynski, and C. Yang, J. Chem. Theory Comput. **13**, 1188 (2017).
[19] S. Chawla and G. A. Voth, J. Chem. Phys. **108**, 4697 (1998).
[20] B. Leimkuhler, D. T. Margul, and M. E. Tuckerman, Mol. Phys. **111**, 3579 (2013).
[21] J. Hutter *et al.*, CPMD: An *Ab Initio* Electronic Structure and Molecular Dynamics Program, see http://www.cpmd.org.
[22] C. Adamo and V. Barone, J. Chem. Phys. **110**, 6158 (1999).
[23] N. Troullier and J. L. Martins, Phys. Rev. B **43**, 1993 (1991).
[24] G. J. Martyna, M. L. Klein, and M. Tuckerman, J. Chem. Phys. **97**, 2635 (1992).
[25] Q. Ma, J. Izaguirre, and R. Skeel, SIAM J. Sci. Comput. **24**, 1951 (2003).
[26] J. Kolafa, J. Comput. Chem. **25**, 335 (2004).
[27] I. Carnimeo, S. Baroni, and P. Giannozzi, Electron. Struct. **1**, 015009 (2019).

Published under license by AIP Publishing